# Deconvolution of Stark broadened spectra for multi-point density measurements in a flow Z-pinch

G. V.  $Vogman^1$  and U.  $Shumlak^2$ 

(Dated: 30 July 2011)

 $<sup>^{1)}</sup>Applied\ Science\ &\ Technology\ Program,\ University\ of\ California,\ Berkeley,\ CA\ 94720$ 

<sup>&</sup>lt;sup>2)</sup> Aerospace & Energetics Research Program, University of Washington, Seattle, WA 98195-2250

Stark broadened emission spectra, once separated from other broadening effects, provide a convenient non-perturbing means of making plasma density measurements. A deconvolution technique has been developed to measure plasma densities in the ZaP flow Z-pinch experiment. The ZaP experiment uses sheared flow to mitigate MHD instabilities. The pinches exhibit Stark broadened emission spectra, which are captured at 20 locations using a multi-chord spectroscopic system. Spectra that are time and chord-integrated are well-approximated by a Voigt function. The proposed method simultaneously resolves plasma electron density and ion temperature by deconvolving the spectral Voigt profile into constituent functions: a Gaussian function associated with instrument effects and Doppler broadening by temperature; and a Lorentzian function associated with Stark broadening by electron density. The method uses analytic Fourier transforms of the constituent functions to fit the Voigt profile in the Fourier domain. The method is discussed and compared to a basic least-squares fit. The Fourier transform fitting routine requires fewer fitting parameters and shows promise in being less susceptible to instrumental noise and to contamination from neighboring spectral lines. The method is evaluated and tested using simulated lines and is applied to experimental data for the 229.69 nm C III line from multiple chords to determine plasma density and temperature across the diameter of the pinch. These measurements are used to gain a better understanding of Z-pinch equilibria.

# I. SPECTROSCOPIC PLASMA DENSITY MEASUREMENTS

Non-perturbing plasma density measurements are important for cases where probes either interfere with the plasma or cannot withstand its temperature. Such non-perturbing methods include laser interferometry,<sup>1–3</sup> Thomson scattering,<sup>4–6</sup> and spectroscopic Stark broadening.<sup>7–13</sup> The use of spectroscopy is particularly convenient since, unlike the other methods, it involves a relatively simple one-time setup, and does not require a beam to enter and exit through multiple ports of an experiment. Likewise many astrophysical measurements are limited to spectroscopic means.

For non-hydrogenic ions the Stark effect gives rise to a Lorentzian spectral profile<sup>13</sup> whose full width at half maximum (FWHM) is directly related to the electron density of the plasma. Spectral lines, whether hydrogenic<sup>7</sup> or non-hydrogenic,<sup>8–10</sup> can be fitted to determine plasma density.<sup>7–11</sup>

The content of this paper investigates the use of Stark broadening as a reliable means of measuring plasma electron density, in parallel with or as an alternative to standard techniques. In particular, a method has been developed to accurately deconvolve Stark and Doppler broadened spectra to simultaneously determine electron density and ion temperature of Z-pinch plasmas at multiple impact parameter locations. In order to distinguish Stark broadening from other forms of broadening, the proposed deconvolution procedure involves line fitting in the Fourier domain, meaning line data and fitting functions are Fourier transformed prior to performing fits. The advantages of this method are that it allows for filtering of contamination from neighboring lines and likewise filtering of signal noise. Resulting fits are therefore more accurate, and can be applied to a larger set of spectral lines, including lines that are not entirely isolated.

# II. DOPPLER AND STARK BROADENING OF SPECTRAL LINES

Chord-integrated emission spectroscopy can be used to measure ion temperature and density using Doppler broadening and Stark broadening, respectively. These broadening effects cause spectral line profiles to change shape and can be treated as being independent of each other.<sup>11,13</sup> The theoretical background associated with spectral line shapes is discussed in detail in Ref. 11. The Doppler effect associated with temperature causes spectral lines to

have a Gaussian profile,

$$G(\lambda) = A_G \exp\left(\frac{-4\ln 2 \cdot (\lambda - \lambda_0)^2}{W_G^2}\right),\tag{1}$$

where  $A_G$  is the amplitude,  $\lambda$  is the wavelength,  $\lambda_0$  is the centroid of a given spectral line, and the FWHM  $W_G$  is defined by

$$W_G = \frac{\lambda_0}{c} \sqrt{\frac{k_B T_i \cdot 8 \ln 2}{m}},\tag{2}$$

where c is the speed of light,  $k_B$  is Boltzmann's constant,  $T_i$  is the ion temperature, and m is the mass of the radiating ion.

Stark broadening in the context of plasmas results from the redistribution of atomic energy levels of a radiating species due to the electric field imposed by surrounding charged particles. Two types of approximations are used depending on the plasma regime of interest. <sup>14,15</sup> In a quasi-static regime, Stark broadening results from the perturbation of a radiator's degenerate states. This perturbation is due to the electrostatic field created by neighboring ions, whose velocity is much less than that of the electrons. The resulting spectral profiles are generally asymmetric. <sup>11,12,14,15</sup>

In the electron impact regime, free electrons perturb the energy levels of the radiating ion, meaning that collisions between electrons and the radiator occur on a time scale that is faster than the decay.<sup>16</sup> The electron impact regime gives rise to symmetric Lorentzian profiles (see Eq. (3)). For the case of non-hydrogenic radiating species, electron impact is the dominant form of broadening.<sup>8,11,13</sup> For most non-hydrogenic ions the Stark effect is quadratic, meaning that the shift in energy levels is proportional to the square of the electric field, which in turn is related to the density through Gauss's Law.<sup>9,10,17</sup>

If the plasma regime falls between the two approximations, either is considered to be sufficiently valid. <sup>18,19</sup> The choice of approximation depends on the relative magnitudes of mean time between collisions and the duration of interaction. <sup>17</sup> For the impurities whose spectra are measured in the ZaP flow Z-pinch experiment, the electron impact approximation best characterizes the plasma regime. The Lorentzian function that describes the Starkbroadened profile can be expressed as

$$L(\lambda) = A_L \frac{W_L^2}{4(\lambda - \lambda_0)^2 + W_L^2},\tag{3}$$

where  $A_L$  is the amplitude, and  $W_L$  is the FWHM, which can be defined in nanometers as<sup>9,10</sup>

$$W_L = 0.2w_e \left(\frac{n_e}{10^{16}}\right) + 0.35\alpha \left(\frac{n_e}{10^{16}}\right)^{1/4} \times \left(1 - \frac{3}{4}N_D^{-1/3}\right) w_e \left(\frac{n_e}{10^{16}}\right)$$
(4)

where  $w_e$  is the tabulated electron impact parameter,  $n_e$  is the electron density in cm<sup>-3</sup>,  $\alpha$  is the ion broadening parameter,  $N_D$  is the number of particles in the Debye sphere. The first term represents electron impact broadening and the second term represents corrections due to line asymmetries. For the case of non-hydrogenic radiators the FWHM is<sup>9,10</sup>

$$W_L = 0.2w_e \left(\frac{n_e}{10^{16}}\right). \tag{5}$$

In order to make quantitative measurements it is critical to perform background subtraction and account for all mechanisms of broadening that are relevant to the experiment and to its instrumentation. This includes accounting for instrument broadening, which is independent of plasma properties, and can be quantified through calibration. Experimentally measured spectra are convolutions of the different broadening effects.<sup>11,17</sup> The convolution of a Lorentzian and Gaussian is given by a Voigt profile,

$$V(\lambda) = \int_{-\infty}^{\infty} G(\lambda - \lambda') L(\lambda') d\lambda'.$$
 (6)

The broadening effects can be characterized by performing numerical fits to the data; a Gaussian function is used to fit purely Doppler-broadened spectral data, <sup>20</sup> a Lorentzian function is used to fit purely Stark broadened spectral data, <sup>10,21,22</sup> and a convolution of the two — i.e. the Voigt profile — is used to fit data that has a combination of the two effects. <sup>9</sup> The FWHMs of the constituent Gaussian and Lorentzian functions are related to temperature and density, respectively, through simple analytic expressions (Eq. (2) and Eq. (5)). It is important to note that the Voigt profile accurately describes spectral broadening for the case of the electron impact regime. Applying a Voigt fit to an asymmetric line can result in temperature and density calculation errors of up to 25%. <sup>12</sup>

# III. SPECTROSCOPIC MEASUREMENTS

The ZaP flow Z-pinch experiment and its hardware are described in detail in Ref. 23. The experiment produces a 1–2 cm diameter plasma column that is 1 m long, has electron densities of  $10^{22}$ – $10^{23}$  m<sup>-3</sup>, and temperatures of 100–200 eV. Radially sheared flows in the plasma allow it to remain stable for 20–60  $\mu$ s, which is orders of magnitude longer than the instability growth time. Accurate measurement of the radial variation of the ion temperature and electron density provide valuable insights on the shear mechanism and plasma stability.

Refs. 24 and 25 describe the spectroscopic instrumentation used on the experiment. In summary, optical fibers collect chord-integrated light along twenty impact parameters across the diameter of the Z-pinch, a 0.5 m Acton Research Spectra Pro 500i spectrometer separates the light based on wavelength, and spectra are recorded with a 512 × 512 pixel intensified charge-coupled device (ICCD). The impact parameters of the twenty fibers span a distance of 34 mm. Since the hydrogen plasmas in ZaP are typically fully ionized, impurity ions are used for most spectroscopic measurements. Of particular interest is the C III 229.69 nm ion line, which is a high-intensity isolated line that is consistently observed in ZaP plasmas.

The spectrometer is equipped with three different gratings, the finest of which is a 3600 grooves/mm grating, which has a wavelength resolution of 0.011 nm/pixel. All of the data presented in this paper are collected using the 3600 grooves/mm grating. The spectrometer and fiber optic system are calibrated using a 1 eV cadmium ion pen lamp, which has an isolated Cd I spectral line at 228.80 nm — close to the C III line of interest. The signal recorded through each of the twenty fibers in response to the lamp is fitted with a Gaussian, which characterizes the instrument broadening, and thus the instrument function for each fiber. The instrument function's FWHM is used to compute the instrument temperature associated with each of the twenty fibers. The instrument temperature, — which is defined using Eq. (2), mass m of a C III ion, and  $\lambda_0$  of 229.69 nm — is an artificial parameter that is used as a convenient means to describe instrument broadening. Table I shows the instrument temperatures associated with each chord.

The convolution of a Gaussian instrument function (with temperature  $T_{inst}$  and FWHM  $W_{G,inst}$ ) and a Doppler profile (with temperature  $T_i$  and FWHM  $W_{G,i}$ ) yields a Gaussian

TABLE I. Instrument temperatures (with uncertainties of  $\pm 2$  eV) associated with each of the twenty optical fibers used to collect spectral data from ZaP plasmas.

Chord #	(1)	(2)	(3)	(4)	(5)	(6)	(7)	(8)	(9)	(10)
T [eV]	34	32	29	27	26	24	21	19	18	17
Chord #	(11)	(12)	(13)	(14)	(15)	(16)	(17)	(18)	(19)	(20)
T [eV]	17	16	15	16	17	19	19	20	21	21

whose FWHM is given by<sup>17</sup>

$$W_{G,eff} = \sqrt{W_{G,i}^2 + W_{G,inst}^2}. (7)$$

In accordance with Eq. (2), the temperatures of the respective profiles are related by:

$$T_{eff} = T_i + T_{inst}. (8)$$

Consequently, the convolution of a Gaussian instrument function and a Doppler profile yields a Gaussian whose FWHM has an effective temperature that is the sum of the instrument temperature and the ion temperature. Thus the values of the effective temperature, which is determined from a fit, and the instrument temperature, which is derived from calibration, can be used to determine the ion temperature.

# IV. NUMERICAL FITS IN THE FOURIER DOMAIN

In order to determine the Lorentzian FWHM, and hence electron density, it is necessary to generate a numerical fit to a given spectral line. Lines with high signal-to-noise ratios are preferred. Prior to fitting, the background — associated with instrument noise and bremsstrahlung radiation — must be subtracted from the spectral data. If both Stark and Doppler effects are present, a Voigt profile is used to fit the data.

When expressed in the form given by Eq. (6), the amplitude,  $W_L$ ,  $W_G$ , and  $\lambda_0$  need to be optimized (e.g. in the least-squares sense) to fit a given spectral line. This is referred to as a "basic fit."

The convolution integral given by Eq. (6) can also be represented by Fourier transforms. Thus the Fourier transforms of a Voigt profile,  $\hat{V}$ , is the product of the Fourier transform of the Gaussian,  $\widehat{G}$ , and the Fourier transform of the Lorentzian,  $\widehat{L}$ , both of which have explicit analytic forms that give

$$\widehat{V}(k) = \widehat{G} \cdot \widehat{L} = A_V \exp\left(-\frac{W_G^2 k^2}{16 \ln 2} - \frac{W_L |k|}{2}\right), \tag{9}$$

where  $A_V$  is the amplitude, and k is the wavenumber. The expression for  $\widehat{V}$  is purely realvalued because the original spectral line data can be translated by  $\lambda_0$  to give a centroid of zero. In the Fourier domain this means that shift factors of  $e^{i\lambda_0 k}$  that would otherwise multiply  $\widehat{G}$  and  $\widehat{L}$  are equal to one. Since all spectral line shape information is contained in Eq. (9), a numerical fit can be performed in the Fourier domain. The fitting of Eq. (9) to the real part of the discrete Fourier transform of the spectral data is referred to as a "Fourier fit." The unknown variables that are to be optimized in the fit are  $W_G$ ,  $W_L$ , and  $A_V$ . For the simple case in which only one type of broadening mechanism is observed, either  $W_G$  or  $W_L$  in Eq. (9) will be zero. The centroid  $\lambda_0$  need not be optimized for the Fourier domain fit. In addition to eliminating a fitting variable, performing the fit in the Fourier domain presents other advantages. In particular, it allows for spectral filtering, making it possible to reduce the effects of signal noise and the impact of contamination from neighboring spectral lines that may overlap with the line of interest.

#### V. ANALYSIS OF SYNTHETIC SPECTRAL DATA

The Fourier fitting method is tested by applying it to synthetic data that are constructed with specified densities and temperatures. The Fourier fit and the basic fit are first applied to ideal Voigt profile data with no added error. For ideal Voigt profile data the Fourier fit offers no advantage over a basic fit, and in fact is slightly less accurate due to additional numerical manipulation involved in fitting. However, real spectral line data have instrumental noise and may often be contaminated by the presence of neighboring lines. Synthetic data was constructed to emulate these effects (see top plot of Fig. 1). For simplicity an instrument temperature of zero is assumed so that the effective temperature is equal to the ion temperature  $T_i$ .

The synthetic spectral data are generated by the superposition of two Voigt profiles with simulated noise. The simulated noise is the superposition of two parts: one part that is proportional to the inverse square root of the intensity and one part that is constant for the

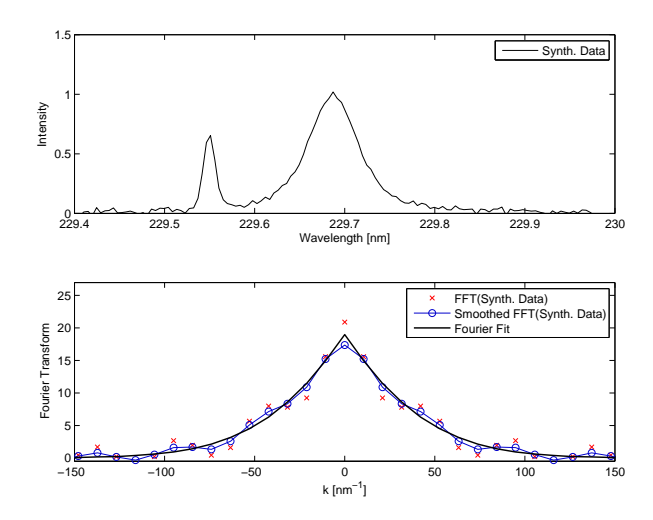


FIG. 1. Synthetic spectral line data (centroid  $\lambda_0$  of 229.69 nm) with a contaminating line (centroid  $\lambda_0$  of 229.55 nm) and simulated error to approximate typical signal noise (top) are Fourier transformed and smoothed (bottom). The parameters  $A_V$ ,  $W_G$ , and  $W_L$  in Eq. (9) are optimized to generate a least-squares fit of the real part of the Fourier-transformed data.

TABLE II. Synthetic data with a contaminating line is fitted using the Fourier fit and a basic fit. The Fourier fit produces a more accurate measure of temperature and density, while the basic fit drastically overestimates the effect of Stark broadening.

	$T_i$ [eV]	$n_e  [{\rm m}^{-3}]$	$W_G$ [nm]	$W_L$ [nm]
Synthetic Data	50	$8.0\times10^{22}$	0.0360	0.0448
Fourier Fit	47	$7.7\times10^{22}$	0.035	0.043
Basic Fit	3	$11.3\times10^{22}$	0.009	0.063

entire domain. The first part represents the standard deviation of the Poisson statistical distribution which describes the photon counts measured by the ICCD. The second part of the noise is an arbitrary instrumental error. The synthetic data (see Fig. 1 and Fig. 2) consist of 129 data points over a wavelength range of 229.39–229.99 nm, a sampling that is representative of real spectroscopic data. Since real data resolution is determined by the number of pixels in the CCD detector and the wavelength span is set by the spectrometer, any given spectrum will have a fixed range of wavelengths and sample points.

The simulated data are fitted with both a Fourier fit and an unweighted basic fit. In order to perform the Fourier fit, the data are first Fourier transformed using a Cooley-Tukey

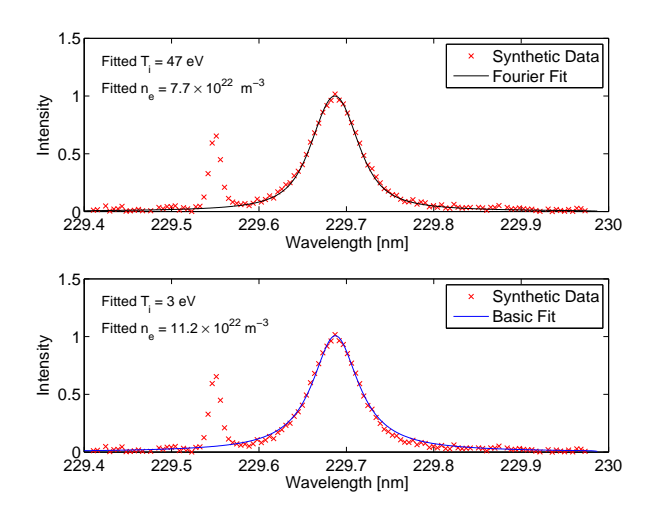


FIG. 2. A least-squares Fourier fit (top) is compared to a least-squares basic fit (bottom). Values of synthetic and fitted parameters are given in Table II. The Fourier fit is better able to resolve the shape of the line of interest.

discrete fast Fourier transform algorithm, for which the number of sample points need not be a power of two. The original synthetic data and its Fourier transform are shown in Fig. 1. The presence of the off-center contaminating line in the synthetic data adds a small amplitude and a high-frequency oscillation to the Fourier-transformed data (see Fig. 1). The added amplitude is highest at wavenumber k=0 and is much less than (in this case  $\approx 5\%$  of) the amplitude associated with the line of interest. The frequency of oscillation is related to the distance between the centroid of the contaminating line and the centroid of the line of interest. To filter out the effect of the contaminating line, the real part of the Fourier-transformed data are smoothed with a 3-point boxcar smoother (see the bottom plot in Fig. 1). The smoothed Fourier-transformed synthetic data are then least-squares fitted using Eq. (9). Table II shows the temperatures, densities, Gaussian FWHMs, and Lorentzian FWHMs for synthetic spectral data, the Fourier fit to the data, and the basic fit to the data. The resulting fits are shown in Fig. 2.

By smoothing and fitting in the Fourier domain, it is possible to eliminate the effects of the contaminating line and noise. Consequently, the Fourier fit better approximates the shape of the line of interest, and yields more accurate ion temperature and electron density estimates. By contrast, the basic fit simply averages over the noise, and is significantly affected by the presence of the contaminating line. The contaminating line causes the basic fit to overestimate the Lorentzian width, and hence the electron density, while underestimating

the Gaussian width and hence the ion temperature (see Table II). While the basic fit might be improved by weighting certain wavelength ranges or larger intensities, the Fourier fitting method eliminates the need to arbitrarily select a wavelength range or intensity cutoff.

In order to determine the range of ion temperatures and electron densities for which the Fourier fit is valid, a combined mean square error — associated with the difference between synthetic data parameter values and fitted parameter values — is calculated for a range of temperatures and densities. The mean square error,  $\epsilon$ , is defined as

$$\epsilon = \sqrt{\left(\frac{n_e^{fit} - \tilde{n}_e}{\tilde{n}_e}\right)^2 + \left(\frac{T_i^{fit} - \tilde{T}_i}{\tilde{T}_i}\right)^2},\tag{10}$$

where  $\tilde{n}_e$  and  $\tilde{T}_i$  are the known values of electron density and ion temperature, and  $n_e^{fit}$  and  $T_i^{fit}$  are the fitted values. The temperature and density errors were also evaluated independent of one another to determine the factors limiting the range of validity of the fit. Synthetic C III data with noise as before, but without a contaminating line, are constructed and fitted for ion temperatures of 1 – 900 eV and electron densities of  $0.15 \times 10^{22}$  m<sup>-3</sup> –  $30 \times 10^{22}$  m<sup>-3</sup>. The combined mean square error (see Eq. (10)) is plotted in Fig. 3, which shows a distinct region over which the error is minimized. Fig. 3 also shows lines of constant  $W_L$  to  $W_G$  ratios.

At sufficiently high densities, and especially densities exceeding  $25 \times 10^{22}$  m<sup>-3</sup>, the Fourier fit cannot accurately resolve temperature. Analogously, for temperatures that exceed 600 eV, the Fourier fit cannot accurately resolve electron density. In effect, independent of the relative magnitudes of  $W_G$  and  $W_L$ , the dominating error at high temperatures is in the density value, and the dominating error at high densities is in the temperature value. As the total FWHM of a spectral line increases, due to either higher temperature or density, the Fourier-transformed profile becomes narrower, thereby decreasing the resolution of the peaked profile in the Fourier domain, and thus decreasing the accuracy of the fit. As seen in Fig. 3, this resolution effect sets a limit on the maximum density and temperatures that can simultaneously be resolved.

Thus for cases in which spectral data are both Doppler broadened and Stark broadened, ion temperatures and electron densities can be accurately resolved using the Fourier fit provided that:  $n_e$  is approximately between  $2 \times 10^{22}$  m<sup>-3</sup> and  $15 \times 10^{22}$  m<sup>-3</sup>;  $T_i$  is approximately between 1 and 500 eV; and the ratio of  $W_L$  to  $W_G$  is between 0.07 and 3 (see Fig. 3). Outside

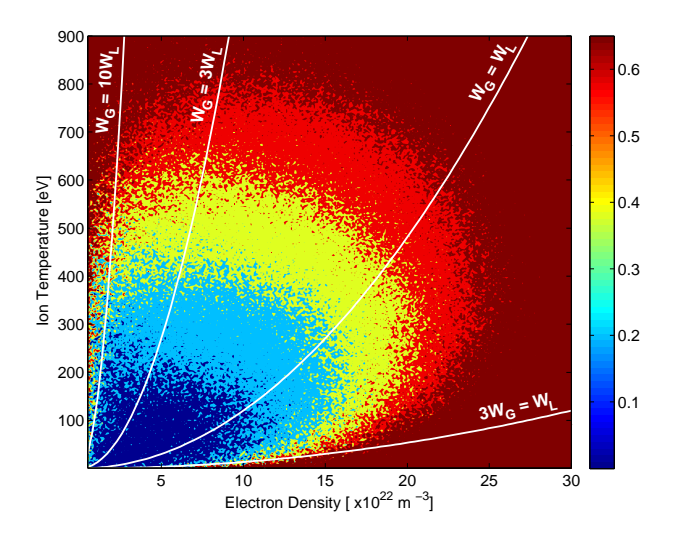


FIG. 3. The combined mean square error, as defined in Eq. (10), for Fourier fits applied to synthetic data with ion temperatures in the range of 1–900 eV and electron densities in the range of  $0.15 \times 10^{22}$ – $30 \times 10^{22}$  m<sup>-3</sup>. Lines of constant FWHM ratios (the ratio of  $W_L$  to  $W_G$ ) are shown in white. The minimum error is seen for densities and temperatures approximately in the range of:  $2 \times 10^{22}$ – $15 \times 10^{22}$  m<sup>-3</sup>, and 10–500 eV. Regions of dark red represent a mean square error of 0.65 or higher.

of these ranges either ion temperature or electron density, but not both, can be accurately resolved. Namely, at low temperatures  $(W_G \ll W_L)$  the spectral profile of interest is assumed to be purely Lorentzian, and analogously for low densities  $(W_G \gg W_L)$  the spectral profile is assumed be purely Gaussian. In cases where one of the two broadening effects is negligible, the range of validity of the fitting technique is vastly increased.

# VI. ANALYSIS OF SAMPLE EXPERIMENTAL DATA

In addition to the synthetic data, the Fourier fitting technique is also applied to C III 229.69 nm spectral line data collected from ZaP plasmas. The C III 229.69 nm line is of particular interest to ZaP since it is a consistently-observed high-intensity line that is isolated from other impurity lines seen in the experiment. The line data, after taking a subset of the available ICCD data, consist of 129 data points on a wavelength range of 228.99–230.44 nm. The line data and the Fourier and basic fits are shown in Fig. 4 for one chord of spectral data, corresponding to chord-integrated impurity radiation at an impact parameter of -13.42 mm

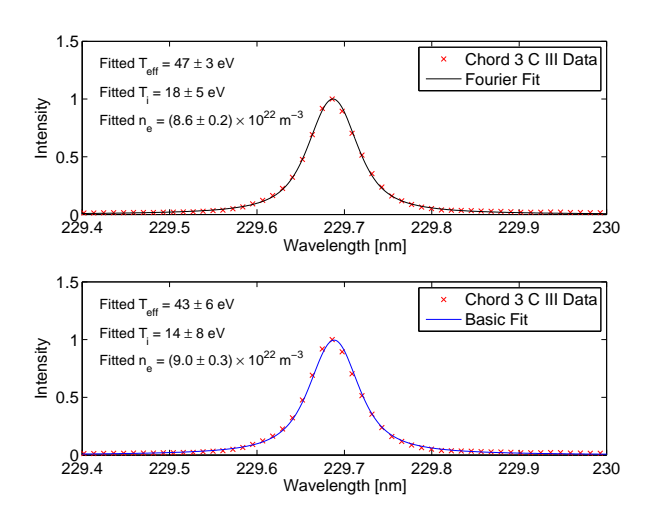


FIG. 4. A Fourier fit (top) and basic fit (bottom) are applied to C III 229.69 nm line data for experimental Pulse 80313017. The two fits yield comparable density and temperature measurements.

from the axis of the experiment. The Fourier fit and basic fit yield electron densities of  $(8.6 \pm 0.2) \times 10^{22} \text{ m}^{-3}$  ( $W_L = 0.048 \pm 0.001 \text{ nm}$ ) and  $(9.0 \pm 0.3) \times 10^{22} \text{ m}^{-3}$  ( $W_L = 0.050 \pm 0.002 \text{ nm}$ ) respectively, indicating that the two fitting methods yield consistent results for the case of isolated lines. The computed density values are also consistent in magnitude with those measured by interferometry<sup>23</sup>; however, the values cannot be directly compared since the spectroscopic and interferometric measurements are averaged differently. Specifically, interferometry measures chord-integrated density, and spectroscopy measures chord-averaged density weighted by the spectral line emission.

The effective temperature, listed as  $T_{eff}$  in Fig. 4, is the sum of the ion temperature  $T_i$  and the instrument temperature. Both the effective temperature and ion temperature values are included for reference. The Fourier and basic fits yield effective temperatures of  $47 \pm 3$  eV ( $W_G = 0.035 \pm 0.001$  nm) and  $43 \pm 6$  eV ( $W_G = 0.033 \pm 0.002$  nm), respectively. The instrument temperature of Chord 3 (see Table I), corresponding to impact parameter of -13.42 mm, is used to compute the ion temperatures for the Fourier and basic fits:  $18 \pm 5$  eV and  $14 \pm 8$  eV, respectively.

In addition to the one chord of data shown in Fig. 4, the data from other chords are used to compute densities and ion temperatures at other impact parameters. The resulting electron density and ion temperature profiles across the diameter of the Z-pinch are shown in Fig. 5 for three experimental pulses. Each point corresponds to a fit that is analogous to the top plot in Fig. 4.

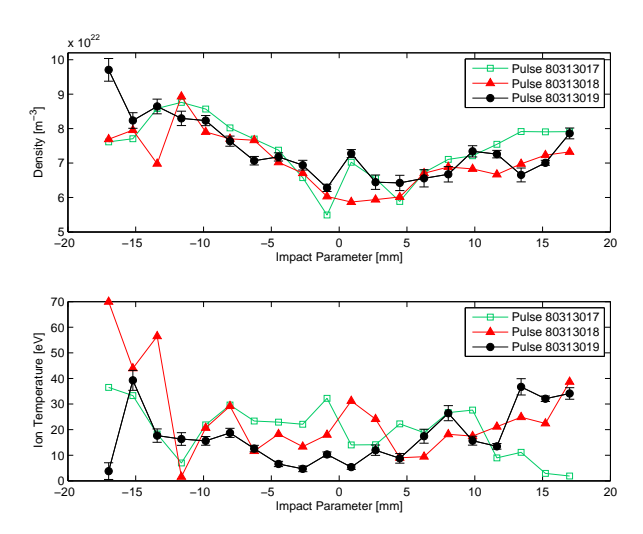


FIG. 5. Average electron density and ion temperature measurements determined using Fourier fits to C III 229.69 nm spectral data at each of twenty chords. The chords span the diameter of the Z-pinch. Uncertainties in the measurements are shown for Pulse 80313019, and are representative of the Pulse 80313017 and Pulse 80313018 uncertainties, which are omitted for clarity.

Uncertainties are defined as 95% confidence intervals for the optimized values of  $W_G$  and  $W_L$ , and by extension  $T_i$  and  $n_e$ . The optimal values  $W_{G,opt}$  and  $W_{L,opt}$  are determined by minimizing the least-squares error (i.e. the sum of the squares of the residuals associated with the fit), which serves as a measure of the accuracy of the fit. Once the optimal values are found, the non-linear dependence of  $W_{G,opt}$  and  $W_{L,opt}$  on the intensity data can be approximated locally as a linear dependence. Using the local linear approximation and assuming the intensity data consists of jointly normal distributions with sample means and sample variances makes it possible to determine the variance of the sought parameters around the mean values  $W_{G,opt}$  and  $W_{L,opt}$ . The uncertainties in ion temperature and electron density, as derived from uncertainties in  $W_G$  and  $W_L$ , are plotted in Fig. 5 for Pulse 80313019, and are representative of the uncertainties calculated for Pulse 80313017 and Pulses 80313018. The error bars for the latter are omitted for clarity.

The fact that the resolved electron density is a chord-averaged measurement and is relatively uniform across the diameter of the pinch indicates that the C III ion is in the outer shell (i.e. outer radius) of the Z-pinch. By applying the Fourier fitting procedure to other ion lines, it would be possible to determine how density varies with the Z-pinch radius.

# VII. CONCLUSIONS

A technique has been developed to resolve plasma electron densities from Stark and Doppler broadened spectral data by performing an optimization fit in the Fourier domain. The technique resolves ion temperature and electron density simultaneously, and can be applied to isolated as well as overlapping lines. Fitting to Fourier-transformed spectral data allows for spectral filtering of noise and contaminating lines, and thereby presents a flexible and accurate means by which to quantify electron density from Stark broadening. The fitting method has been applied to synthetic data and experimental C III line data. The results are consistent with synthetic data inputs and with experimental interferometric measurements.

By extending the set of spectral data that can be fitted, the Fourier method makes density measurements more accessible. In particular, electron impact plasma regimes with densities that range between  $2 \times 10^{22}$  m<sup>-3</sup> and  $15 \times 10^{22}$  m<sup>-3</sup>, and effective temperatures between 1 eV and 500 eV can be accurately resolved using the Fourier fit. Because spectral data are easier to collect than interferometric and Thomson scattering data, the proposed fitting technique presents useful diagnostic information for plasma electron densities.

# ACKNOWLEDGMENTS

The authors would like to acknowledge the valuable conversations with J.A. Morrow on the topic of convolutions. In addition, the authors would like to recognize that this research was supported by the U.S. Department of Energy under Grant No. DE-FG02-04ER54756. The research was also supported in part by the Department of Energy Office of Science Graduate Fellowship Program (DOE SCGF), made possible in part by the American Recovery and Reinvestment Act of 2009, administered by ORISE-ORAU under contract no. DE-AC05-06OR23100.

# REFERENCES

<sup>1</sup>M.A. Van Zeeland, R.L. Boivin, T.N. Carlstrom, T. Deterly, and D.K. Finkenthal, Review of Scientific Instruments **77**, 10F325 (2006).

<sup>2</sup>B.V. Weber and D.D. Hinshelwood, Review of Scientific Instruments **63**, 5199–5201 (2009), ISSN 0034-6748.

- <sup>3</sup>L.M. Smith, D.R. Keefer, and N.W. Wright, Review of Scientific Instruments **74**, 3324 (2003).
- <sup>4</sup>J.W. Hughes, D.A. Mossessian, A.E. Hubbard, E.S. Marmar, D. Johnson, and D. Simon, Review of Scientific Instruments **72**, 1107 (2001).
- <sup>5</sup>S. Hassaballa, M. Yakushiji, Y.K. Kim, K. Tomita, K. Uchino, and K. Muraoka, Plasma Science, IEEE Transactions on **32**, 127–134 (2004).
- <sup>6</sup>A. Kono and K. Nakatani, Review of Scientific Instruments **71**, 2716 (2000).
- <sup>7</sup>V.A. Soukhanovskii, D.W. Johnson, R. Kaita, and A.L. Roquemore, Review of Scientific Instruments **77**, 10F127 (2006).
- <sup>8</sup>H.R. Griem, Physical Review **128**, 515–523 (1962).
- <sup>9</sup>A. Ionascut-Nedelcescu, C. Carlone, U. Kogelschatz, D.V. Gravelle, and M.I. Boulos, Journal of Applied Physics **103**, 063305 (2008).
- <sup>10</sup>S.S. Harilal, C.V. Bindhu, R.C. Issac, V.P.N. Nampoori, and C.P.G. Vallabhan, Journal of Applied Physics 82, 2140 (1997).
- $^{11}\mathrm{V}.$  Milosavljević and G. Poparić, Phys. Rev. E  $\mathbf{63},\,036404$  (Feb 2001).
- <sup>12</sup>N. Konjevi, Physics reports **316**, 339–401 (1999).
- <sup>13</sup>H.R. Griem, Physica Scripta **1999**, 142 (1999).
- <sup>14</sup>D. Salzmann, Atomic physics in hot plasmas (Oxford University Press, USA, 1998).
- <sup>15</sup>F.E. Irons, Journal of Physics B: Atomic and Molecular Physics **6**, 1562 (1973).
- <sup>16</sup>W.F. Mahmoudi, N.B. Nessib, and S. Sahal-Bréchot, Physica Scripta **70**, 142 (2004).
- <sup>17</sup>I.H. Hutchinson, *Principles of Plasma Diagnostics* (Cambridge Univ Pr, 2002).
- $^{18}\text{H.R.}$  Griem and K.Y. Shen, Physical Review **122**, 1490–1496 (1961).
- <sup>19</sup>P.C. Kepple and H.R. Griem, Physical Review A **26**, 484 (1982).
- <sup>20</sup>D.W. Auerbach, D.N. Hill, and H.S. McLean, Tech. Rep. (Lawrence Livermore National Laboratory (LLNL), Livermore, CA, 2001).
- <sup>21</sup>L. Godbert, A. Calisti, R. Stamm, B. Talin, S. Glenzer, H.J. Kunze, J. Nash, R. Lee, and L. Klein, Physical Review E 49, 5889–5892 (1994).
- $^{22}\mathrm{G.S.}$  Yun, S. You, and P.M. Bellan, Nuclear Fusion 47, 181 (2007).
- <sup>23</sup>U. Shumlak, C.S. Adams, J.M. Blakely, B.J. Chan, R.P. Golingo, S.D. Knecht, B.A. Nelson, R.J. Oberto, M.R. Sybouts, and G.V. Vogman, Nuclear Fusion 49, 075039 (2009).
- <sup>24</sup>D.J. Den Hartog and R.P. Golingo, Review of Scientific Instruments 72, 2224 (2001).
- $^{25}\mathrm{R.P.}$  Golingo and U. Shumlak, Review of Scientific Instruments 74, 2332 (2003).

<sup>26</sup>P.R. Bevington, and D.K. Robinson *Data Reduction and Error Analysis for the Physical Sciences* (McGraw-Hill Higher Education, 2003).

